Nonlinear electromagnetic vibration energy harvester comprising dual helical-plane springs and multiple Halbach arrays for low-frequency and small-amplitude vibrations

Zhongsheng Chen[1,2*], Zhiwen Chen[2], Yongxiang Wei[2], Yeping Xiong[3]

[1] College of Automotive Engineering, Changzhou Institute of Technology, Changzhou, China

[2] College of Electrical and Information Engineering, Hunan University of Technology, Zhuzhou, China

[3]Faculty of Engineering and Physical Sciences, University of Southampton, SO16 7QF, UK

* Corresponding author: chenzs@czu.cn

Abstract: Electromagnetic vibration energy harvesters are widely investigated for self-powered wireless sensors and nonlinearity has been introduced for low-frequency and broadband vibration energy harvesting. But how to realize the nonlinearity with small amplitudes, high reliability and few complexities is still a challenge in real-world applications. In this paper, a novel electromagnetic vibration energy harvester comprising dual helical-plane springs and multiple Halbach arrays is proposed. The structural characteristics are analyzed, which indicate that the helical-plane springs can have nonlinear stiffness under small-amplitude vibrations and multiple Halbach arrays can greatly enhance the magnetic field. Then a magnet-electro-mechanical model is built by combining mechanical dynamics &electrodynamics, which is numerically solved by using the Runge-Kutta algorithm. Finally, the feasibility of the nonlinear electromagnetic vibration energy harvester is validated both numerically and experimentally. The results show that it has a nonlinear stiffness, a resonance bandwidth of 3Hz and a peak power of 14mW when the excitation amplitude is only 0.5g. In particular, the resonance frequency range depends on the excitation amplitude. Furthermore, the prototype of a self-powered wireless temperature sensor is constructed and testified. The results of this study indicate that the proposed structure can be utilized and extended to build compact, reliable and nonlinear electromagnetic vibration energy harvesters for low-frequency, small-amplitude and broadband vibrations in real-world applications.

Keywords: Self-powered wireless sensors; Electromagnetic vibration energy harvester; Nonlinearity; Helical-plane springs; Multiple Halbach arrays

1. Introduction

Nowadays, wireless sensor nodes (WSNs) have been widely used in the field of Internet of Things (IoT) [1], such as industrial condition monitoring, environmental protection, agriculture monitoring, and so on. These WSNs can be used to sample various parameters including temperature, humidity, pressure, light intensity, etc. Then these sampled data will be transmitted to remote cloud servers for analysis and storage. In order to achieve

long-term operation, it is very necessary to provide reliable and stable power supplies for WSNs. At present, electrochemical batteries are typically used to power WSNs. However, conventional batteries generally have a limited lifetime, so it always needs to replace these batteries. In many cases, battery replacement is either too difficult or too costly [2]. In order to address this issue, WSNs usually need to be self-powered. That is to say, they need to harvest electric energy from the surrounding environment to drive their own operation. Energy harvesting (EH) has becomes a research hot spot in the field of IoT [3]. Depending on the application and the place of WSNs, different kinds of environmental energy can be harvested, for example, solar [4], thermal [5] or vibration energy [6]. In particular, vibration energy is an advantageous power source alternative due to the large ambience of vibrations in the real world [7]. Vibration energy can be converted into electricity by using different working principles [8-10]. Up to now, vibration energy harvesters (VEHs) are typically divided into piezoelectric [11, 12], electrostatic [13], electromagnetic [14-16], and triboelectric categories [17, 18].

As for powering WSNs in real-world applications, VEHs have to face several requirements. The first one is from small volume and light weight. There is always no redundant space to hold a large or heavy VEH due to the requirement of compact design. Moss et al. [19] reviewed scaling and power density metrics of electromagnetic vibration energy harvesters. Gardonio and Bo [20] gave a theoretical study on the scaling laws of linear electromagnetic and piezoelectric VEHs. Elliott and Zilletti [21] discussed the relationship between the efficiency of an electromagnetic harvester and its size by using a non-dimensional electromagnetic coupling coefficient. The second one is from small amplitude and low frequency. Vibration control is often carried out to reduce the harm to the host structures or devices, so vibration amplitudes are small. The third one is from reliability. VEHs should have a long-term life in order to maintain the WSNs. Under considering these requirements, electromagnetic vibration energy harvesters (EVEHs) are more suitable than other types due to the advantages of large output current, long service life and low cost. In particular, EVEHs mainly use the relative motion between solid magnets and coils, so they have strong resistance to harsh environments, leading to higher reliability. Thus EVEHs have been extensively investigated by both academia and industry. Muscat et al. gave an overview of EVEHs [16]. Early researches have mostly focused on linearly resonant EVEHs [22, 23]. In this case, the output power of a linear EVEH can reach the maximum value only when its resonance frequency matches the dominant frequency of the environmental vibration. Otherwise, the output power will drop significantly once the excitation frequency deviates from the resonance condition. Unfortunately, environment vibrations are mostly broadband, so a linear EVEH has limited performance in real-world applications. An ideal EVEH should be able to generate high power output across a wide frequency spectrum. In order to address this

issue, the introduction of nonlinearities into EVEHs has attracted wide attention in the past decades [24-27].

Nonlinearity in VEHs can take on various forms according to the literature. Jia [28] has reviewed and compared eight major types of nonlinear mechanisms that have previously been reported in the field of VEH, which include Duffing nonlinearity, bistability/multi-stability, parametric resonance, stochastic resonance, mechanical frequency conversion, mechanical end-stop effect, self-tuning mechanism and non-oscillatory mechanism. Similarly, these nonlinear mechanisms can also be introduced for EVEHs. By now, many studies have been carried out on nonlinear EVEHs and the results demonstrate that such nonlinear EVEHs often outperform traditional linear ones. In most existing works, nonlinearity in EVEHs comes from the spring term, including third-order [29] and high-order [30] polynomial springs. But it can be found out that most works mainly focus on theoretical modeling &analysis based on dynamic equations, while prototyping investigations are less done. The difficulty lies in how to realize the nonlinear spring for real-world applications. Traditional springs have nonlinear characteristics under large deformations, which are only suitable for large-amplitude vibrations. In addition, mechanical stoppers will cause physical impacts, leading to structural fatigue, wear and tear. In recent years, magnetic springs have been widely used to form nonlinear spring, where the cantilever-like [31] or levitation-like [32] structures are often built by using opposing magnets on either ends. However, these kinds of structures with more magnets may easily lead to a higher volume and a lower power density. Moreover, magnetic springs will likely generate high-order nonlinearity which is difficult to be stably controlled. Thus how to achieve the nonlinearity with low amplitudes, high reliability and few complexities is still a challenge of utilizing EVEHs in real-world applications.

According to the literature, planar springs can display stiffening behaviors and achieve a noticeable bandwidth enhancement. Therefore, few scholars began to study planar springs for nonlinear EVEHs. Sui et al [33] studied four different planar springs with the permanent magnet attached on the center of the spring and the resonance frequencies were larger than 150Hz. Aiming at MEMS-based EVEH, Sun et al. [34] proposed to tune the thickness to length ratio of the planar spring for tuning linear and nonlinear stiffness coefficient separately and the resonance frequencies were larger than 400Hz. It can be found in the above works that a single planar spring is often used for the EVEH and the resonance frequency is large. In real-world applications, however, the vibration frequencies are always less than 50Hz. In addition, the Halbach array is an array of permanent magnets arranged to produce a very strong magnetic field on one side and practically cancel it on the other side [35]. It can decrease the resonance frequency and increase greatly the harvested power in a compact volume. At the same time, the way of using a single planar spring with Halbach arrays will lead to instability during vibrations.

Ismardi et al. [36] had a try on double planar spring for EVEH, but only finite element analysis (FEA) was done. Therefore, the objective of this paper is to design and realize a reliable nonlinear EVEH for efficiently harvesting small-amplitude, low-frequency and broadband vibration energy. To deal with it, the main contribution of this paper is to present a novel nonlinear EVEH with two structural features of dual helical-plane springs and multiple Halbach arrays. The remainder of this paper is organized as follows: In Section 2, structural characteristics of the proposed nonlinear EVEH is analyzed, including the nonlinear stiffness and the magnetic field. In Section 3, a magnet-electro-mechanical model of the EVEH is built by combining mechanical dynamics and electrodynamics. Then the response of the harvester is numerically derived by integrating the Runge-Kutta algorithm and the effects of key parameters are investigated in Section 4. Experiments are done to validate the proposed EVEH in Section 5. In the end, some conclusions are marked in Section 6.

2. Structural analysis of the proposed nonlinear EVEH

2.1 Description of basic architecture

The schematic 3D structure of the proposed nonlinear EVEH is shown in Fig.1(a), which is mainly composed of dualhelical-plane springs, four identical Halbach arrays & the holder, eight identical coils &bobbins, mechanical supports and the harvesting circuit. The eight coils are divided into four groups and connected in series. The four Halbach arrays are placed in the holder and suspended between the top and bottom helical-plane springs, leading to the Halbach-spring assembly as shown in Fig.1 (b). In the EVEH, all coils are fixed to the frame and the Halbach-spring assembly can vertically move inside these coils. When the EVEH is excited by an external vibration, there will be relative motions between the Halbach arrays and the coils. Therefore, vibration energy can be converted into electrical energy according to the Faraday's law of electromagnetic induction.

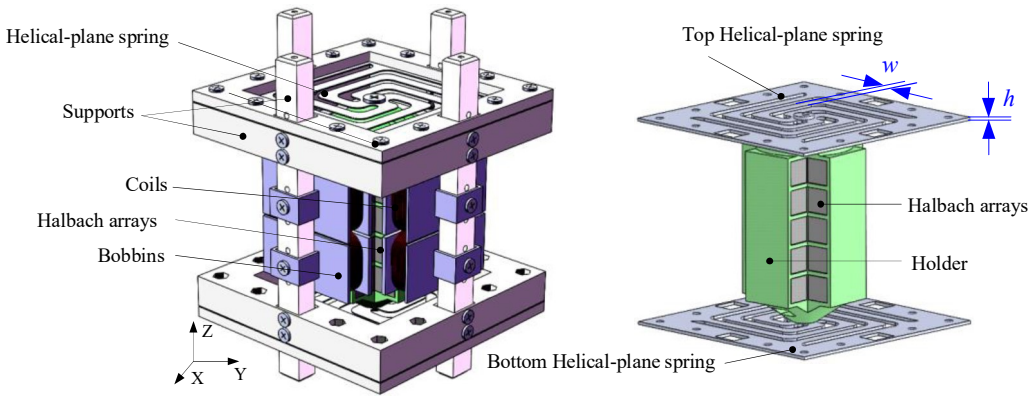

(a) The whole view (b) The Halbach-spring assembly

Fig. 1. The architecture of the proposed nonlinear EVEH

Major advantages of Halbach arrays are that they can typically enhance the magnetic field intensity and

reduce the overall volume of the EVEH. Also rectangular Halbach arrays have been widely used in the literature. Here, the four identical rectangular Halbach arrays are configured as Fig.2 in order to keep compact and each Halbach array is formed by five block NdFeb magnets. The gap between the coil and the magnetic is equal to *d*. In this way, the magnetic field on the outer side can be greatly enhanced. In addition, the resonance bandwidth of a linear EVEH with traditionally linear springs is often narrow, so that broadband vibration energy is hardly harvested effectively. Therefore, the planar spring is adopted here. Meanwhile, if only a helical-plane spring is used, the Halbach-spring vibrator may produce lateral motion which will directly result in unexpected collision and friction with the coil. To deal with this issue, this paper proposes to adopt dual helical-plane springs, which are connected to the two terminals of the Halbach arrays. Furthermore, modal analysis of the Halbach-spring assembly is done and the first four mode shapes and frequencies are shown in Fig. 3. It can be seen that: i) The dominant mode shape is the first-order vertical motion and the contribution of other mode shapes is much small; ii) Other mode frequencies are much more than the first-order one, so the magnet-spring assembly mainly keep vertical motions under low-frequency vibrations.

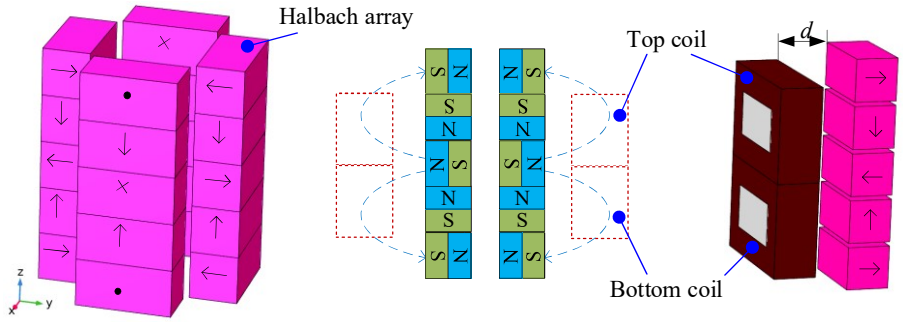

(a) The four rectangular Halbach arrays (b) Magnetic field lines (c) The Halbach-coil pair

Fig.2. Spatial configuration of the Halbacharrays and coils

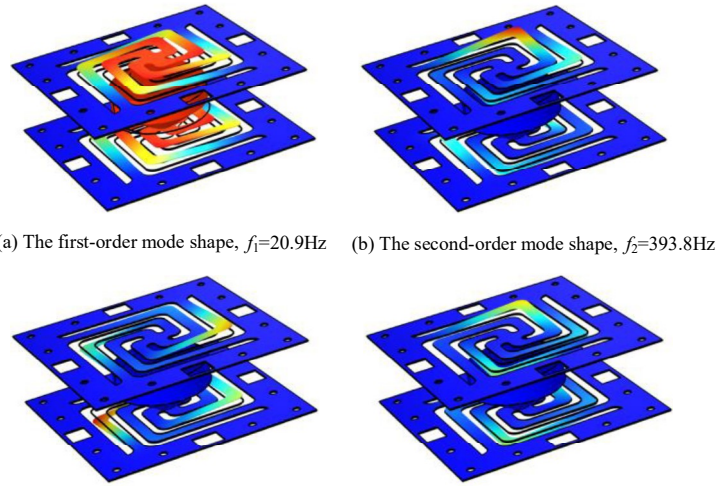

(a) The first-order mode shape, f_1=20.9Hz (b) The second-order mode shape, f_2=393.8Hz

(c) The third-order mode shape, f_3=394.1Hz (d) The fourth-order mode shape, f_4=396.2Hz

Fig 3. The first four mode shapes and frequencies of the Halbach-spring assembly

In summary, the advantages of the proposed nonlinear EVEH can be sorted into four aspects. The first one is *Simplicity*. The whole harvester is just composed of several simple mechanical components and has no complex parts. The second one is *Compactness*. Instead of using magnetic springs, the utilization of planar springs makes the Halbach-spring structure be compact. The third one is *Reliability*. The structure comprising dual helical-plane springs has no collision and friction between the Halbach arrays and the coils, so that the harvester can work reliably for long time. The fourth one is *Nonlinearity*. The overall stiffness of the dual helical-plane springs can be nonlinear under small vibrations, so nonlinearity will be introduced to enhance low-frequency and broadband vibration energy harvesting. As we all know that the performance of an EVEH depends strongly on the spring characteristics, the magnetic characteristics and the coil characteristics. Therefore, FEA will be next done to investigate these characteristics.

2.2 The natural frequency of the Halbach-spring assembly

According to Fig.3, the first-order mode frequency is important since it denotes the resonance frequency. In order to carry out low-frequency VEHs, the harvester should be designed to make the resonance frequency be as small as possible. The Halbach-spring assembly is simulated in the COMSOL software. Here the helical-plane spring with size 45×45 mm^2 is made from Steel and the size of each NdFeb magnet is $5\times5\times10$mm^3.

As we all know that the natural frequency depends on the equivalent mass and stiffness. Here the equivalent mass is fixed for given Halbach arrays. Therefore effects of key spring parameters on the natural frequency will be simulated. At the same time, the helical-plane spring has four cantilevers with a width of w and a thickness of h. Then the effects of h and w on the natural frequency are shown in Fig 4. It can be seen that the natural frequency increases with both h and w. That is to say, it needs to reduce h and w in order to generate low resonance frequency. In turn, however, reducing h or w will decrease the strength of the cantilever, which may shorten the service life. Thus there should be a tradeoff between the resonance frequency and the reliability in actual applications.

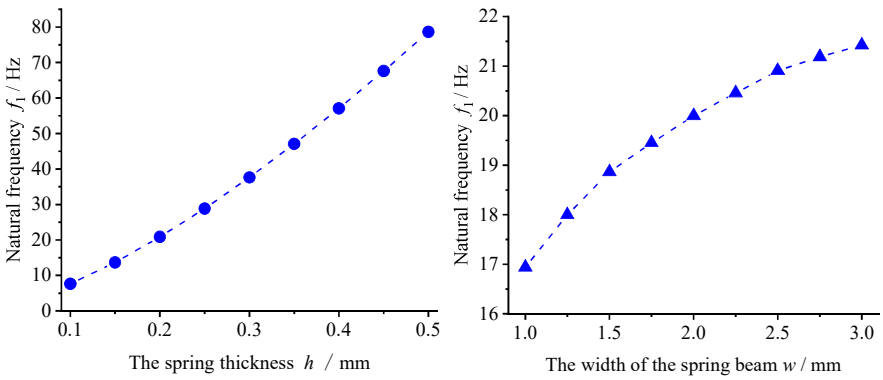

Fig 4.The natural frequency v.s. (a) h and (b) w

2.3 Potential nonlinearity of the dual helical-plane springs

As stated before, nonlinearity is an effective solution to realize broadband vibration energy harvesting. Thus it is much significant to investigate potential nonlinearity of the dual helical-plane springs. Analytical formula is difficult to get, so FEA-based static simulations are done to find the relationship between the restoring force and the elastic deformation. The process can be summarized into four steps: Firstly, the Halbach arrays with the holder are looked as an equivalent mass. The entity models of the dual helical-plane springs and the equivalent mass are built in the SolidWorks software, which are then imported into the COMSOL software. Secondly, both material properties and boundary constraints are set. Thirdly, a static force acts on the top of the equivalent mass and the displacement of the bottom of the equivalent mass is equal to elastic deformation. Finally, the parametric sweep analysis is done to obtain the relationship between the force and the elastic deformation. The relationship curves with different h and w are shown in Fig. 5, respectively. One can see that: i) In Fig. 5(a), the width w is fixed as 2.5mm. When h becomes small, the stiffness tends to be nonlinear. While h is large enough, the stiffness should be linear; ii) In Fig. 5(b), the thickness h is fixed as 0.2mm. The stiffness tends to be nonlinear with the increase of w. Moreover, the nonlinearity increases with w. Thus both small h and large w are desirable to enhance the nonlinearity of the dual helical-plane springs, but in turn reduce the reliability and increase the resonance frequency according to Fig. 4. Therefore, there is also a tradeoff between the nonlinearity and the reliability in actual applications.

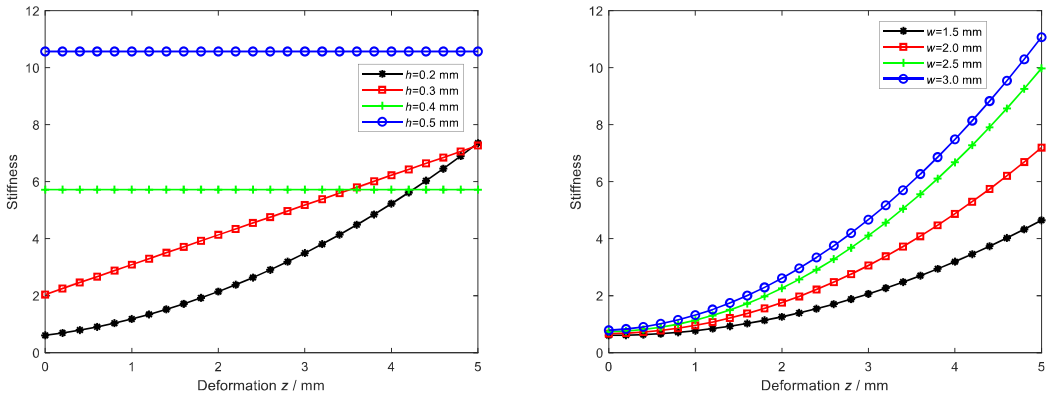

Fig.5. The stiffness characteristics with different (a) h and (b) w

Furthermore, the nonlinear spring can be modeled as the hardening-spring Duffing oscillator by referring to the literature [37]. That is to say, the relationship between the restoring force ($F_e(z)$) and the elastic deformation ($z = z(t)$) can be represented as,

$$F_e(z) = \alpha z + \beta z^3 \tag{1}$$

where α, β are the fitting coefficients. For different h and w, these fitting coefficients are calculated and listed in Table 1 by using FEA. Then the nonlinear stiffness of the dual helical-plane springs can be written as,

$$k_{nl}(z) = \alpha + 3\beta z^2 \tag{2}$$

Table 1 Estimations of fitting coefficients for different geometric parameters

Geometric parameters	α	β
w=2.5mm, h=0.2mm	609.5	6.45×10^7
w=2.5mm, h=0.3mm	2364	1.93×10^8
h=0.2mm, w=1.5mm	435.5	7.34×10^6
h=0.2mm, w=2.0mm	539.2	4.45×10^7
h=0.2mm, w=3.0mm	859.5	1.45×10^8

2.3 Magnetic characteristics of the four Halbach arrays

Magnetic characteristics play an important role of the nonlinear EVEH. Firstly, the four Halbach arrays as Fig. 2(b) are modeled in the COMSOL software and geometric parameters (magnet length, magnet width, magnet thickness and magnet spacing) of each Halbach array is defined in Fig. 6(a) and Table 2. The x, y and z axis are shown in Fig. 6(b). Next, the magnetic flux density of the four Halbach arrays is calculated and both the cross-section and top views are plotted as Fig. 6(b). It can be easily seen that the magnetic flux density on the outer side is much more than that inside. Also the magnetic field distribution of each Halbach array is almost independent of others. Furthermore, taking the cross section for analysis, the magnetic flux densities at y=4mm (Inside) and y=11mm (Outside) are calculated and shown in Fig. 6(c), respectively. One can see that the magnetic flux densities are symmetric along the z axis and the peak value of the former is almost five times that of the latter, which testifies that the Halbach arrays can enhance greatly the magnetic field.

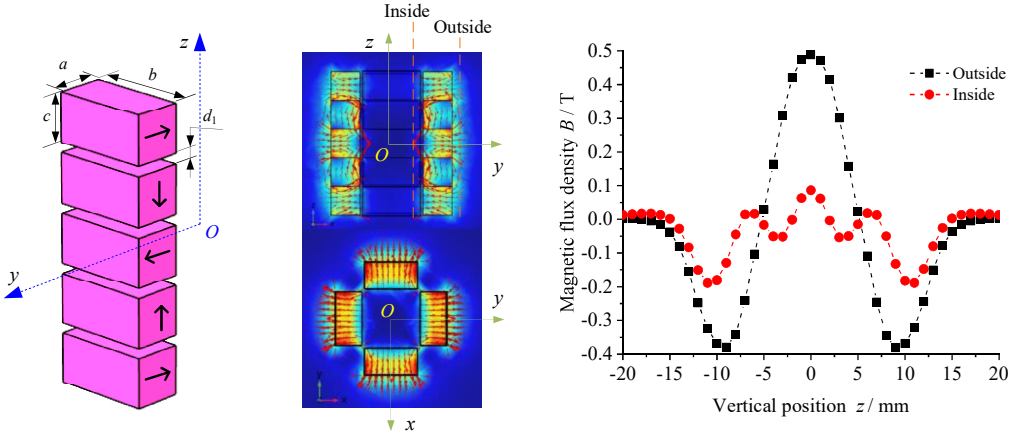

(a) Geometric parameters (b) FEA results (c) Magnetic flux density

Fig. 6 Magnetic field distribution of the Halbach arrays by FEA

Table2 Physical parameters of the Halbach array

Parameter	Value	Parameter	Value
a	5mm	*b*	10mm
c	5mm	Br	1.41T

At the same time, magnetic characteristics of the four Halbach arrays are strongly related to the geometric parameters. In particular, the magnetic gap (d_1) is an important parameter. As for differentd_1, the magnetic flux density at y=12mm is calculated and shown in Fig. 7. It can be seen that both the peak value and the change rate of the magnetic flux density will decrease with d_1. Thus the arrangement of the magnet stack should be as compact as possible when designing the Halbach array.

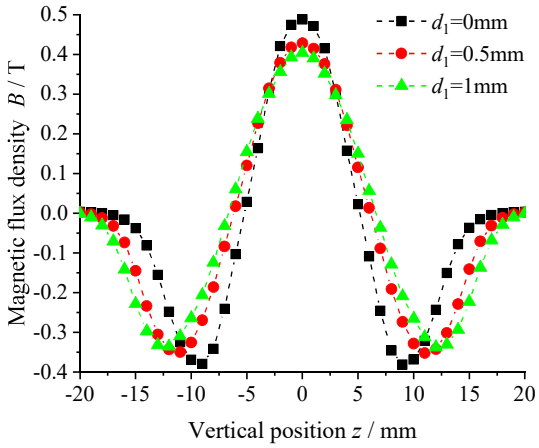

Fig.7. Magnetic flux densities under different d_1

3. Magnet-electro-mechanical model of the nonlinear EVEH

In order to investigate dynamic behavior and the harvesting performance, it needs to build the magnet-electro-mechanical model of the nonlinear EVEH. Nowadays, the lumped-parameter modeling method is widely adopted in the field of magnetic vibration energy harvesting due to the simplicity [38]. Thus the nonlinear lumped-parameter model in Fig. 8(a) is adopted to represent the EVEH, including the equivalent mass (M), the nonlinear stiffness (k_{nl}), the mechanical damping (c_m) and the ampere force (F_{emf}). In theory, c_m is mainly due to air resistance and mechanical friction. F_{emf} is the inverse force generated by the induced current in the coils, which is also called as the electromagnetic shunt damping(c_e) force. The excitation displacement is denoted as $u(t)$ and the vertical displacement of the equivalent mass is denoted as $v(t)$. Then the relative displacement can be written as $z(t)=v(t)-u(t)$.

At the equilibrium position, the center plane of the top-bottom coil coincides with that of the Halbach arrays,

which is set as the datum plane. Meanwhile, the initial deformation of the spring is not considered due to small mass. The overall force diagram of the equivalent mass is shown in Fig.8 (b). Then the dynamic equation can be derived as,

$$M\ddot{z}(t)+c_m\dot{z}(t)+F_{emf}+F_e(z)+Mg=-M\ddot{u}(t) \tag{3}$$

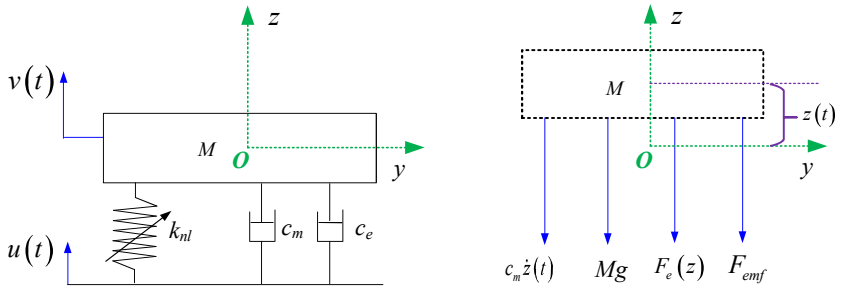

Fig.8. (a) Lumped-parameter model and (b) the force diagram of the equivalent mass

In order to validate the nonlinear EVEH, it needs to analyze its vibration responses. For the sake of simplicity, the electric load is assumed to be a pure resistor (R_L), which can be utilized to observe the harvested power and the bandwidth without loss of generality. Then the electrodynamic equation of the harvesting circuit can be written as,

$$\sum_{j=1}^{8}U_j(t)-\sum_{j=1}^{8}L_j\frac{di(t)}{dt}-\sum_{j=1}^{8}R_ji(t)-R_Li(t)=0 \tag{4}$$

where U_j , R_j and L_j are the induced voltage, the internal resistance and the inductance of the *j*th coil, respectively. $i(t)$ denotes the induced current in the coils. At the same time, the inductance L_j is much small when the excitation frequency is low. In this case, the voltage drops across the inductances will be neglected in the following steps.

According to the reference [39], the ampere force and the induced voltage by the eight coils can be represented as follows, respectively.

$$F_{emf}=c_ei(t)=\eta_{em}i(t) \tag{5}$$

$$U_{out}=\sum_{j=1}^{8}U_j(t)=\eta_{em}\dot{z}(t) \tag{6}$$

where η_{em} denotes the total electromagnetic coupling factor of the eight coils and U_{out} denotes the output voltage.

Combining Eqs.(2)~(6), the magnet-electro-mechanical model of the nonlinear EVEH can be represented as,

$$\begin{cases}M\ddot{z}(t)+c_m\dot{z}(t)+\eta_{em}i(t)+Mg+F_e(z)=-M\ddot{u}(t)\\ \eta_{em}\dot{z}(t)-(R_I+R_L)i(t)=0\end{cases} \tag{7}$$

where $R_I = \sum_{j=1}^{8} R_j$ and M is equal to the sum of the masses of all magnets and the holder. Finally, the harvested power is calculated as $P_h = U_{\max}^2 / R_L$, where $U_{\max}$ is the amplitude of U_{out}.

i) Calculation of the internal resistance of the eight coils (R_I)

The resistance of air cored coils can be calculated once the copper fill factor of the winding process is given. The eight coils are identical, so it only needs to estimate the internal resistance of one coil. Geometric configuration of the coil and the bobbin is shown in Fig. 9. Here the copper fill factor is denoted as k_c. Then the resistance of the eight coils can be approximated as follows.

$$R_I = \frac{4k_c\left(l_3 + l_4 + l_5 + l_6\right) l_1 l_2 \rho_{coil}}{\pi r_{coil}^4} \tag{8}$$

where r_{coil} indicates the wire diameter and ρ_{coil} indicates the wire resistivity.

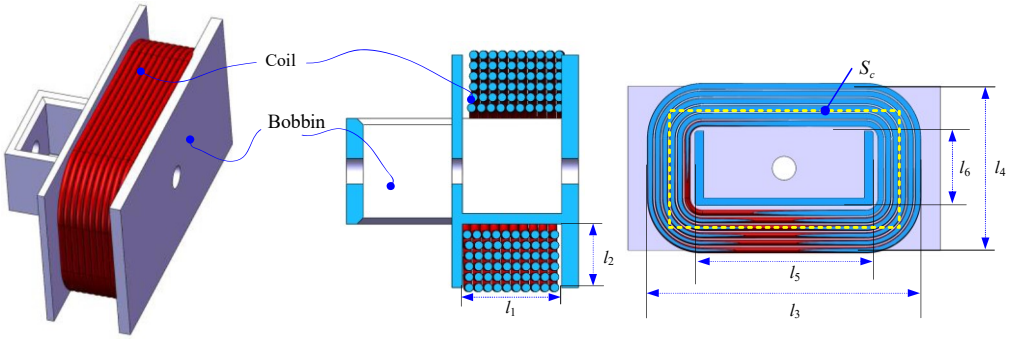

Fig. 9. Geometric configuration of the coil and the bobbin

2) Calculation of the total electromagnetic coupling factor (η_{em})

According to Fig.(6), the four pairs of Halbach-coil are identical and independent, so only a Halbach-coil pair including the top and bottom coils is selected as an example. The magnetic flux of each coil is calculated as

$$\Phi = N_c \iint_A B dA \tag{9}$$

where A indicates the area enclosed by the coil winding, N_c indicates the number of turns and B is the magnetic flux density. But here the analytical calculation of B is rather complicated. Thus B at each vertical position is assumed to be a constant, which is equal to the average magnetic flux density ($B_{avg}\left(z(t)\right)$) going through the coil winding with the area of S_c (S_c is the average area of magnetic flux). Then the induced voltage of the top (or bottom) coil can be represented as,

$$U = -\frac{d\Phi}{dt} \approx -N_c S_c \frac{dB_{avg}}{dz}\dot{z} \tag{10}$$

Based on Eq. (10), the electromagnetic coupling factor of each coil can be calculated as,

$$\eta = -N_c S_c \frac{dB_{avg}}{dz} \tag{11}$$

Furthermore, FEA is adopted to estimate B_{avg} and the parameters of single coil winding are listed in Table 3. For different d, B_{avg} of top and bottom coils are simulated and plotted in Fig.10. It can be seen that: i) The peak value and the gradient of B_{avg} tends to decrease with the increase of d, so small d is desirable for the EVEH; ii) The B_{avg} of the top coil is anti-symmetric to that of the bottom coil, so their electromagnetic coupling factors and induced voltages have opposite signs; iii) When the vertical displacement ($z(t)$) is small, $B_{avg}(z(t))$ can be considered to change linearly. Otherwise, it will be nonlinear. Based on the above simulation results, it is very important to explain how the eight coils are connected in series. That is to say, the bottom coil is inversely connected to the top coil, so that the electromagnetic coupling factors and induced voltages of the eight coils have the same sign, respectively. In this case, it only needs to obtain the average magnetic flux densities of the top and bottom coils in order to estimate the total electromagnetic coupling factor (η_{em}).

Table3 Parameters of single coil winding

Parameter	Value	Parameter	Value
l_1	4.0 mm	l_4	10mm
l_2	2.5mm	l_5	11mm
l_3	17mm	l_6	5.0 mm
r_{coil}	0.1mm	k_c	0.5
ρ_{coil}	0.0185Ω.mm^2/m	N_c	500
S_c	105mm^2		

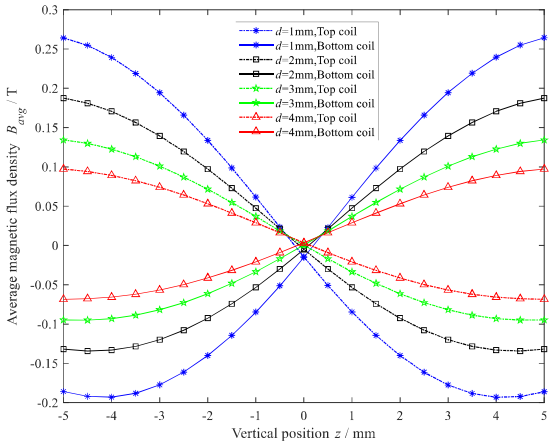

Fig. 10. Estimations of the average magnetic flux density by FEA

Based on the FEA results, a third-order polynomial is used to fit the average magnetic flux densities of the top ($B_{avg}^{T}(z(t))$) and bottom ($B_{avg}^{B}(z(t))$) coils as follows.

$$B_{avg}^{T}\left(z\left(t\right)\right)=\lambda_{10}+\lambda_{11}z\left(t\right)+\lambda_{12}z^{2}\left(t\right)+\lambda_{13}z^{3}\left(t\right) \tag{12a}$$

$$B_{avg}^{B}\left(z\left(t\right)\right)=\lambda_{20}+\lambda_{21}z\left(t\right)+\lambda_{22}z^{2}\left(t\right)+\lambda_{23}z^{3}\left(t\right) \tag{12b}$$

where λ_{10} □ λ_{23} denotes the fitting coefficients, which are estimated and listed in Table 4.

Table4.Fitting coefficients of the average magnetic flux density

d	λ_{10}	λ_{11}	λ_{12}	λ_{13}	λ_{20}	λ_{21}	λ_{22}	λ_{23}
1.0 mm	-0.012	-72.20	2159	1.11×10^{6}	-0.012	72.16	2185	-1.10×10^{6}
2.0 mm	-0.003	-49.94	1325	7.30×10^{5}	-0.003	49.94	1325	-7.30×10^{5}
3.0 mm	0.002	-34.96	784.8	4.89×10^{5}	0.002	34.96	784.8	-4.89×10^{5}
4.0 mm	0.004	-24.84	455.5	3.35×10^{5}	0.004	24.84	455.5	-3.35×10^{5}

Then the total electromagnetic coupling factor of the eight coils can be approximated as

$$\eta_{em}=-4N_{c}S_{c}\left[\left(\lambda_{11}-\lambda_{21}\right)+2\left(\lambda_{12}-\lambda_{22}\right)z\left(t\right)+3\left(\lambda_{13}-\lambda_{23}\right)z^{2}\left(t\right)\right] \tag{13}$$

So far, the magnet-electro-mechanical model in Eq.(7) can be built by substituting Eq. (2), Eq. (8) and Eq. (13) into Eq. (7).

4. Numerical investigations on the nonlinear EVEH

Generally speaking, it is much difficult to get the analytical solution of Eq. (7). Therefore, the response of the nonlinear EVEH will be numerically derived by using the Runge-Kutta algorithm. Moreover, the proposed harvester in this paper is designed for small-amplitude, low-frequency and broadband vibrations. Therefore, the excitation is assumed to be a harmonic vibration with small amplitude and low frequency. Then the sweep-frequency simulation is done to investigate frequency responses of the nonlinear EVEH and validate the broadband characteristics. Without loss of generality, the excitation acceleration is further expressed as $\ddot{u}\left(t\right)=a_{0}\cos2\pi f_{0}t$, where a_{0} indicates the amplitude and f_{0} indicates the excitation frequency. Denoting $q_{1}\left(t\right)=z\left(t\right)$ and $q_{2}\left(t\right)=\dot{z}\left(t\right)$, then Eq. (7) can be transformed into the following state-space equation.

$$\begin{cases}\dot{q}_{1}\left(t\right)=q_{2}\left(t\right)\\ \dot{q}_{2}\left(t\right)=-a_{0}\cos\left(2\pi f_{0}t\right)-g-\left(\left(c_{m}+\dfrac{\eta_{em}^{2}\left(q_{1}\left(t\right)\right)}{\left(R_{I}+R_{L}\right)}\right)q_{2}\left(t\right)+F_{e}\left(q_{1}\left(t\right)\right)\right)\Big/M\\ \eta_{em}\left(q_{1}\left(t\right)\right)q_{2}\left(t\right)-i\left(t\right)\left(R_{I}+R_{L}\right)=0\end{cases} \tag{14}$$

And the initial conditions are represented as,

$$\begin{cases}q_{1}\left(0\right)=z\left(0\right)=0\\ q_{2}\left(0\right)=\dot{z}\left(0\right)=0\end{cases} \tag{15}$$

Next the effects of key geometric parameters on the performance of the nonlinear EVEH will be studied and other simulation parameters are selected as: $M = 41\text{mg}$, R_I=395.2 Ω, R_L=395 Ω, w=2.5mm. Nowadays, it is very difficult to model the mechanical damping equation of a structure. Then c_m is determined as $c_m = 0.14\ \text{N}\cdot\text{s}/\text{m}$ by referring to similar structures in the literature. It must be pointed out that the output voltage is defined as the open-circuit voltage when R_L is set to be much larger than R_I.

4.1 Effect of the spring thickness (h)

As stated before, the thickness (h) of the helical-plane spring is an important parameter. By setting d=2mm and $a_0 = 0.5\text{g}$, the effects of h on the vibration amplitude, the open-circuit voltage (R_L=2 MΩ) and the harvested power are simulated and plotted in Fig.11, respectively. It can be seen that: i) As h increases, the resonance frequency of the nonlinear EVEH also increases; ii) Under the same excitation amplitude, the vibration amplitude of the nonlinear EVEH tends to decrease as h increases. At the same time, however, both the open-circuit voltage and the harvested power will increase. The reason may be that the natural frequency increases with h, so that the open-circuit voltage and the harvested power are also raised according to the theoretical formula.iii) As h increases, the resonance frequency band of the nonlinear EVEH tends to decrease, which shows that nonlinearity can be utilized to enlarge the operating frequency band of the nonlinear EVEH. Furthermore, the above results are also consistent with the FEA results in Fig.4 and Fig.5.

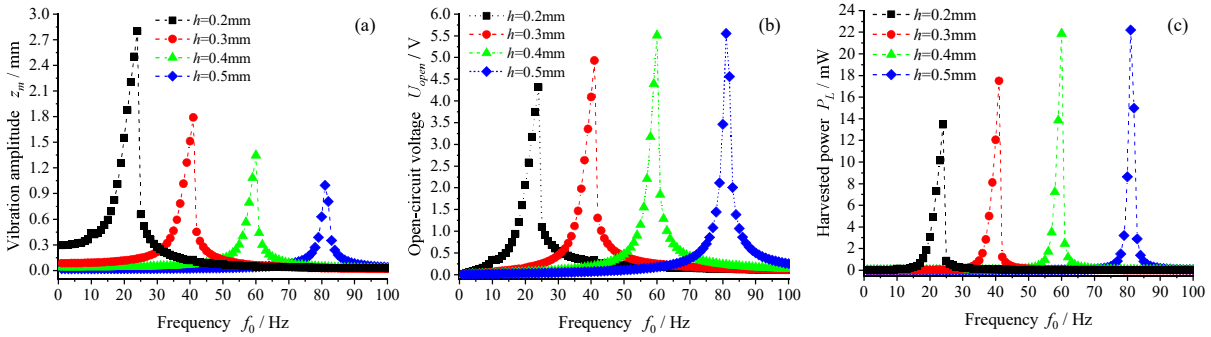

Fig.11.Frequency responses of the (a) vibrationamplitude, (b) open-circuit voltage and (c) harvested power under different *h*.

4.2 Effect of the gap (d)

The gap (d) between the Halbach array and the coil is also an important parameter. By setting $a_0 = 0.5g$ and $h = 0.2\text{mm}$, the effects of d on the vibration amplitude, the open-circuit voltage and the harvested power are simulated and plotted in Fig.12, respectively. It can be seen that: 1) d has little effect on the resonance frequency and the bandwidth; 2) As d increases, both the open-circuit voltage and the harvested power tends to decrease. The reason may be that the electromagnetic coupling factor is large for small spacing. Therefore, small d can be

adopted to enhance the performance of the EVEH.

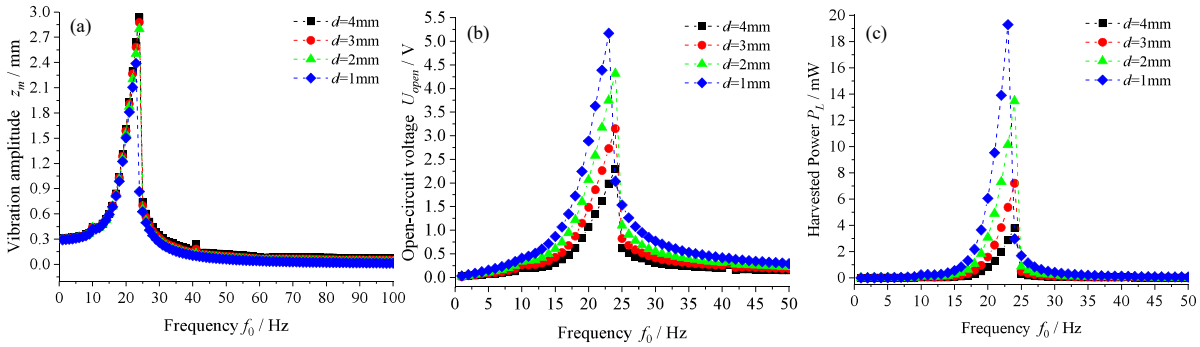

Fig.12. Frequency responses of the (a) vibration amplitude, (b) open-circuit voltage and (c) harvested power under different *d*.

4.3 Effect of the vibration amplitude (a_0)

Besides of the geometric parameters, it is also worthwhile to study the effects of the acceleration amplitude (a_0) on the vibration amplitude, the open-circuit voltage and the harvested power. The simulation results are shown in Fig. 13 and we can see that: i) When a_0 is relatively small, the EVEH tends to be linear. In this case, , the vibration amplitude, the open-circuit voltage and the harvested power achieve the maximum value when the excitation frequency is equal to 21Hz. That is to say, the EVEH resonates with the vibration excitation; ii) When a_0 is relatively large, the frequency response curve bends to the right. Also the vibration amplitude, the open-circuit voltage and the harvested power increase obviously. At the same time, the resonance frequency band also increases; iii) When a_0=0.5g , the peak harvested power is about14mW and the resonance bandwidth is about 3Hz. In particular, the resonance frequency range changes with the excitation amplitude, which can improve the environmental adaptability of the nonlinear EVEH.

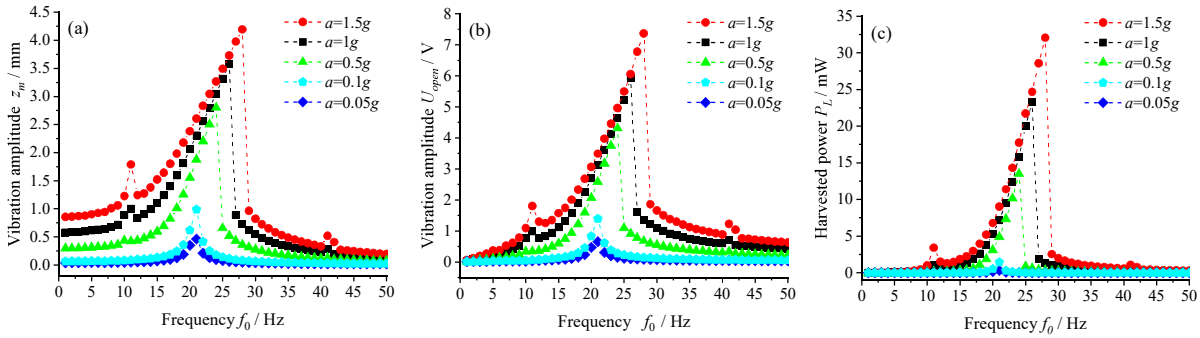

Fig.13. Frequency responses of the (a) vibration amplitude, (b) open-circuit voltage and (c) harvested power under different a_0 .

4.4 Dynamic responses of the nonlinear EVEH

By setting d=2mmand h=0.2 mm, dynamic responses of the nonlinear EVEH under different excitations are calculated and shown in Fig.14, respectively. It can be seen that: i) When $a_0 = 0.1\text{g}$ and $f_0 = 21\text{Hz}$, the EVEH tends to be linear, so that the responses of the vibration displacement, the open-circuit voltage and the harvested power are almost periodic in Fig. 14(a). While $a_0 = 1.5\text{g}$ and $f_0 = 25\text{Hz}$, the EVEH is strongly nonlinear, so that the responses of the vibration displacement, open-circuit voltage and the harvested power are all quasi-periodic (see the 'Nonlinear' in Fig. 14(b)). The results show the nonlinear behaviors. Furthermore, the open-circuit voltage and the harvested power of the equivalent linear EVEH without considering the nonlinear term are also plotted in Fig. 14(b) (see the 'Linear'). It can be seen that the proposed nonlinear EVEH is much superior to the linear one, which also shows that nonlinearity can indeed improve the performance of the EVEH.

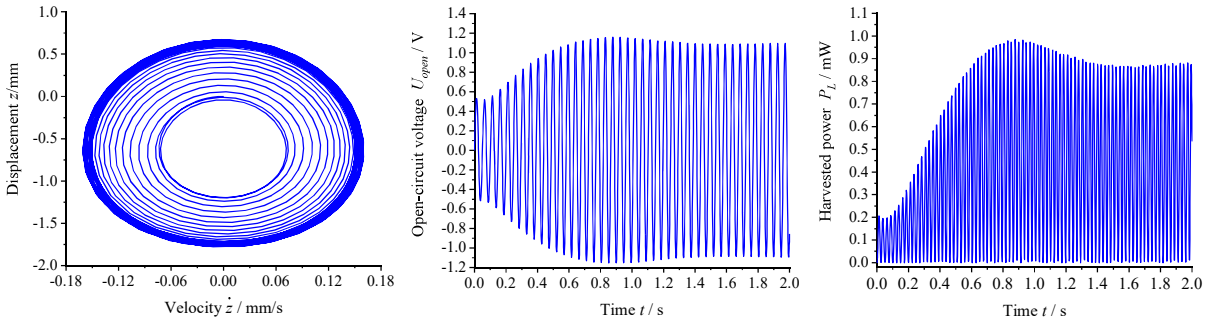

(a) $a_0 = 0.1\text{g}$, $f_0 = 21\text{Hz}$

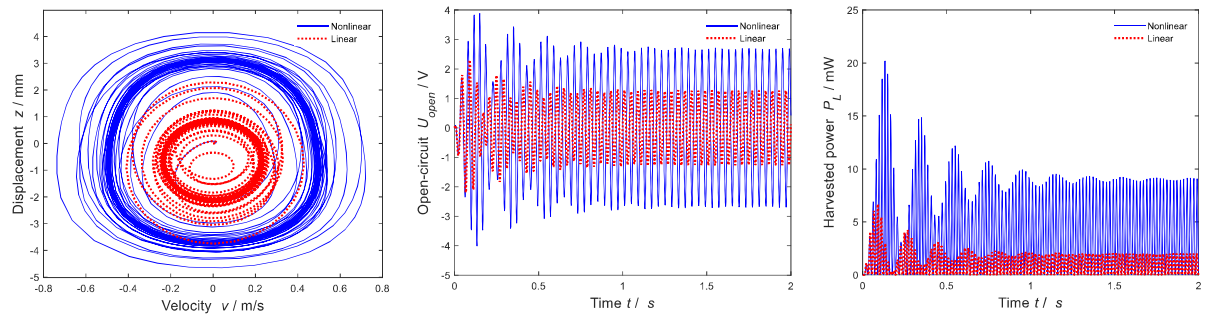

(b) $a_0 = 1.5\text{g}$, $f_0 = 25\text{Hz}$

Fig.14.Dynamic responses of the vibration displacement, the open-circuit voltage and the harvested power

5. Experimental testing and discussions

5.1 Experiment set-up

In order to validate the theoretical results, an experimental set-up is built as Fig.15, which is composed of a signal generator, a power amplifier, an electric shaker, vibrator, a laser vibrometer, a digital oscilloscope and a data acquisition system. The signal generator is used to generate low-frequency and sweep-frequency signals. After being amplified by the power amplifier, the electric shaker is driven to generate the vibration excitation

that acts on the EVEH. The output voltage is observed and sampled by the digital oscilloscope and the excitation vibration is measured by the laser vibrometer. Referring to the theoretical optimization results, the nonlinear EVEH prototype is build and its detailed parameters are listed in Table 2 and Table 5.

Table 5 Detailed values of experimental parameters

Parameter	value	Parameter	value
R_1	323Ω	M	42mg
R_L	320Ω	d	2mm
h	0.2mm	r_{coil}	0.1mm
w	2.5mm	d_1	1mm

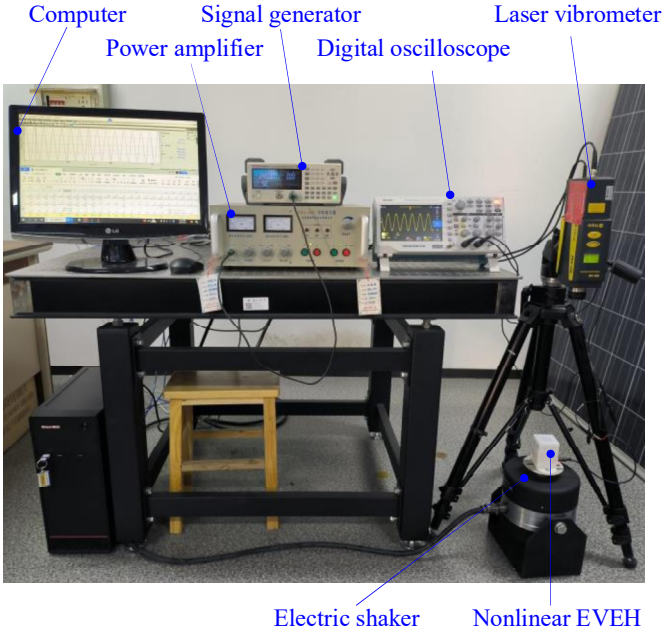

Fig. 15.Experimental set-up

5.2 Measurement of the open-circuit voltage and the harvested power

In the experiment, the up-frequency sweep testing with the step of 1Hz is carried out for given a_0 and f_0. As for each excitation frequency, the corresponding peak values of the open-circuit voltage and the harvested power are recorded and then plotted in Fig. 16. It can be seen that: i) The experimental results are close to the numerical results in Fig.13(b)-(c), which verifies the accuracy of the theoretical model and the corresponding numerical calculation method. At the same time, the deviation of amplitude may be due to the reasons that hand-made coils are not ideal and some assumptions are made in the modeling process; ii) When $a_0 \geq 0.5\mathrm{g}$, both the open-circuit voltage and the harvested power increase greatly. Meanwhile, the response curves bend to the right, leading to wider resonance frequency band; iii) When $a_0 \geq 1\mathrm{g}$, two additional local peaks appear at the frequencies of about 10Hz and 42Hz, which are the same as those appeared in Fig.13. The reason is that nonlinearity can lead to

sub-harmonic and sup-harmonic responses. Furthermore, when a_0=1.5g , the open-circuit voltages and the harvested power under f_0=21Hz , f_0=25Hz and f_0=42Hz are sampled and shown in Fig. 17. It can be interestingly seen that the response frequencies are equal to the excitation frequencies under both f_0=21Hz and f_0=25Hz . But it is not the case under f_0=42Hz , where the response frequency is equal to 21Hz. It further proves the occurrence of the sub-harmonic response. In summary, the above results fully testify that the proposed EVEH is much fit for low-frequency and broadband vibration energy harvesting.

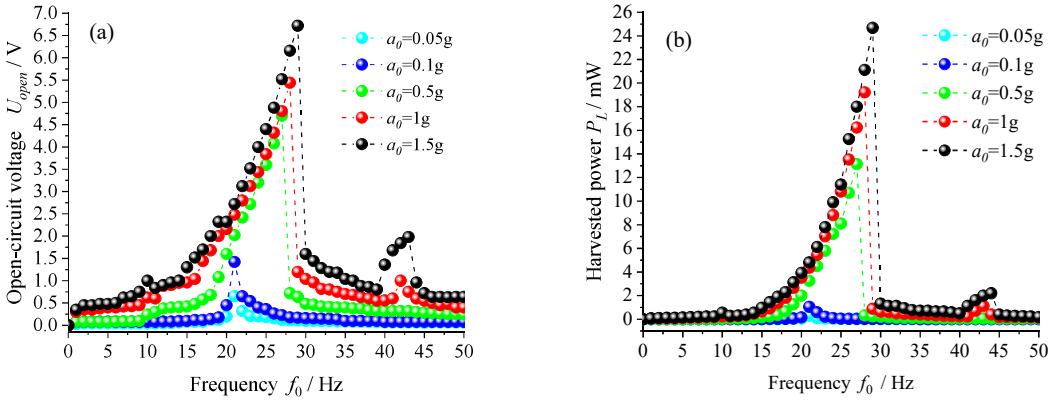

Fig.16 Measured frequency responses of the open-circuit voltage and the harvested power under different a_0

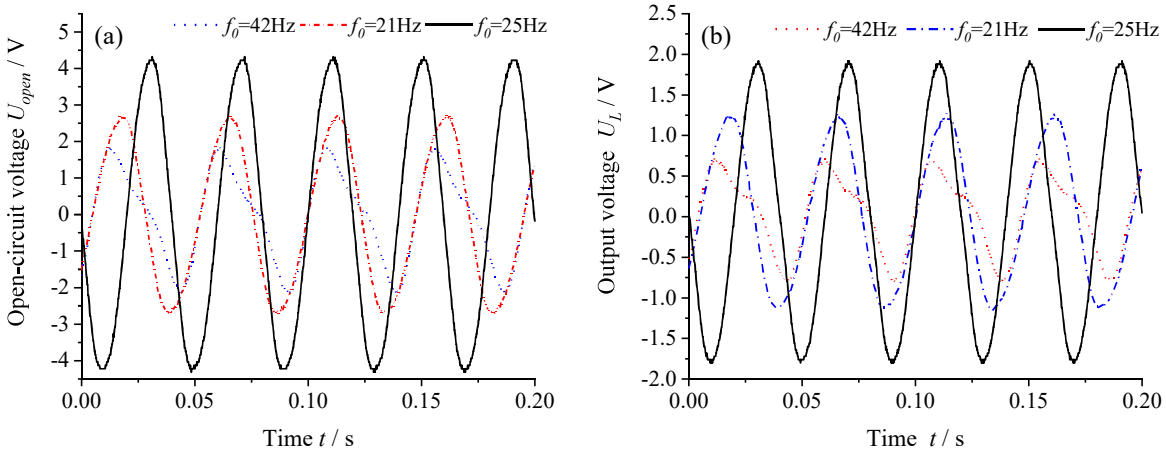

Fig.17. Measured waveforms of (a) open-circuit and (b) output voltages under different f_0

5.3 Prototype of a self-powered wireless temperature sensor and testing

As we all know that the output of the nonlinear EVEH is an AC voltage, so it needs to convert the AC voltage to a DC voltage. In order to validate the feasibility of using the proposed EVEH to power a wireless sensor, an energy conversion & management circuit should be designed. Here the classical bridge rectifier is adopted for energy conversion (e.g. AC-DC). The energy management module is designed based on the chip (BQ25570) and the schematic diagram is shown as Fig. 18(a), which has two key functions of energy storage and delivery. In particular, there is an electric switch in the energy management module, which is designed to control energy

delivery to the electric load. The electric switch is placed between the energy management module and the self-powered wireless temperature sensor module. When the voltage across the storage capacitor is large than the work voltage of the wireless temperature sensor, the switch is on. Then the sensor wakes up and begins to work. Once the voltage across the storage capacitor is less than the work voltage of the sensor module, the switch is off. Then the sensor enters into the sleep mode. Thus the low-power wireless temperature sensor works in an intermittent mode. By integrating the proposed EVEH and the energy conversion & management circuit, the prototype of a self-powered wireless temperature sensor is made as Fig. 18(b), which is called as the self-powered temperature sensor.

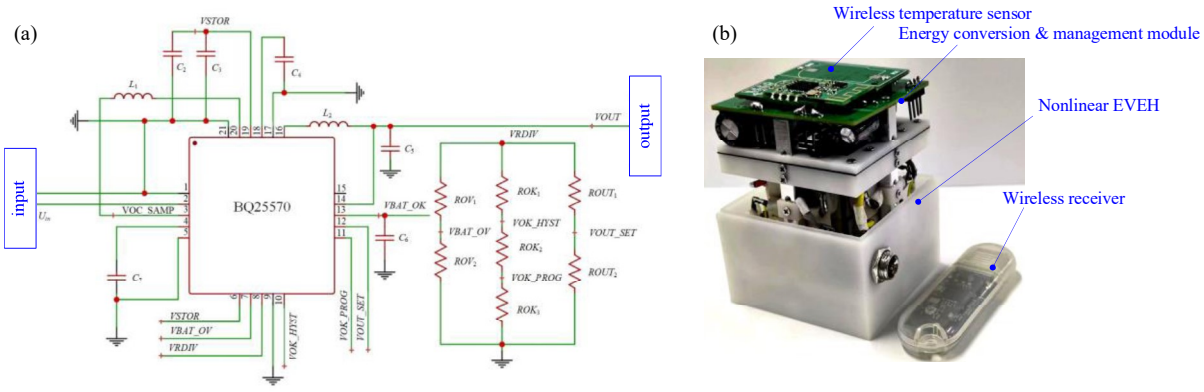

Fig. 18. Picture of the self-power temperature sensor with the nonlinear EVEH

In the experiment, the vibration excitation is set as $a_0 = 0.5\text{g}$ and $f_0 = 22\text{Hz}$. The output of the nonlinear EVEH is directly connected to the self-powered temperature sensor. Then the voltage (U_s) across the storage capacitor and the output voltage (U_{out}) are recorded for analyzing the procedure of energy storage and delivery, which are shown in Fig.18 respectively. It can be seen that: i) The voltage U_s changes periodically from 2.8V to 4.26V. The reason is that 2.8V and 4.26V are set as the lower and upper threshold of the electric switch, respectively. That is to say, the switch turns on and the EVEH provides electric power for the sensor when $U_s > 4.26\text{V}$. When $U_s < 2.8\text{V}$, the switch turns off and the EVEH is disconnected from the sensor. ii) Once the switch turns on, U_s drops instantly from 4.2V to 3.4V and U_{out} increases instantly from 0.5V to 3.0V. There is a voltage drop (0.4V) between U_s and U_{out}, which is generated by the electric switch and the sensor; iii) After the switch turns on, both U_s and U_{out} rise in a short time and then drops oscillatingly. This is because the sensor is waked up from the sleep mode during the short time and the power consumption is very small. In this case, the internal resistance-capacitor loop of the energy conversion & management circuit will continue to charge the storage capacitor. Once the sensor begins to work, the power consumption will increase, so both U_s and U_{out} drop; iii) Under the given vibration excitation, the EVEH cannot power the sensor continuously, which

demonstrates that the instantaneous power of the EVEH is less than the power consumption of the sensor. Therefore it is necessary to accumulate electric energy; iv) The working cycle of the sensor is about 53 seconds and the duty cycle is about 0.3. The stored energy in one cycle is enough to ensure that temperature signals can be collected and transmitted for eleven times. Furthermore, if the number of signal transmission is reduced, the working cycle will be shortened. In summary, the above testing results fully testify that the wireless temperature sensor can be self-powered by the proposed EVEH under low-frequency and small-amplitude vibrations.

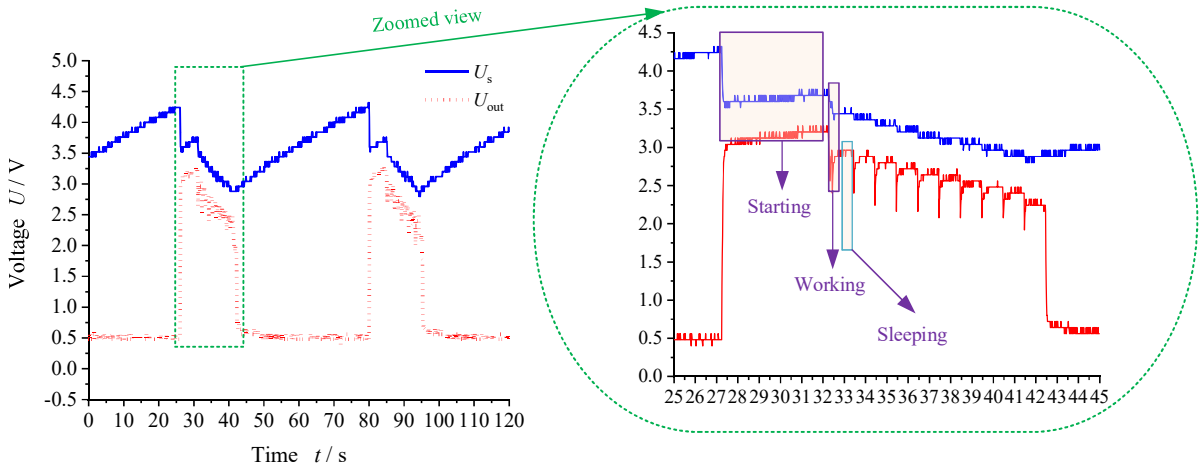

Fig. 19. Measured waveforms of U_s and U_{out}

5.4 Reliability analysis of experimental results

During the experimental process, there are mainly two classes of errors: measurement errors and structural errors. As for measurement errors, the whole testing process is relatively simple. The excitation including the frequency sweep is automatically generated by the signal generator. The vibration signals are collected from the accelerator sensors. The voltage signals are monitored and sampled by the digital oscilloscope. In the experiment, the accelerator sensors have also been calibrated well. At the same time, each testing has been repeated for several times during experiments. Therefore, the measurement errors should be relative small enough to have little effect on the system's responses, which can be testified by that Eq. 13 is much similar to Fig. 16.

As for structural errors, there are indeed several influencing factors. The first one is the geometrical parameter, including the size of each element, the gap between the coil and the Halbach arrays. Due to manufacturing errors, the errors of geometrical parameters are unavoidable. The second one is the magnet's residual magnetism. The real Br is not exactly equal to 1.41T due to manufacturing errors. The third one is the coil winding which is made by hand. In this case, the structure of the coil is not ideal. During the experiments, the EVEH prototype are designed and assembled carefully in order to reduce the structural errors as possible. Actually, some small errors can be found between the simulation parameters and the experimental parameters in this paper. Also Fig. 13 is

not exactly the same as Fig. 16. All these indicate the difference between theoretical and experimental results. At the same time, however, it must be pointed out that the difference between theoretical and experimental results is relatively small, such as Fig. 13 and Fig. 16. In summary, the above experimental results are credible.

6. Conclusions

Although nonlinear EVEHs have been widely investigated for low-frequency and broadband vibrations, it is much necessary to realize the nonlinearity with small amplitudes, high reliability and few complexities in real-world applications. To meet this challenge, a EVEH comprising dual helical-plane springs and multiple Halbach arrays is investigated in this paper. Finally, numerical simulations and experiments were done to validate the proposed structure. Main highlights of this paper may include: i) It is evident that the dual helical-plane springs exhibit nonlinear stiffness under small-amplitude vibrations, which is directly related to the cantilever's thickness and width; ii) The magnetic field distribution of each Halbach array is autonomous, so that employing multiple Halbach arrays can considerably amplify the magnetic field; iii) Effect of key parameters on the performance of the proposed nonlinear EVEH is revealed, which will provide guidelines for designing in real-world applications; iv) Compared with existing cantilever-like or levitation-like nonlinear structures using magnetic springs, the dual helical-plane springs can generate nonlinearity within small volumes. Therefore the proposed harvester in this paper is more compact than them. The results of this study indicate that the proposed structure can be utilized to realize self-powered wireless sensors in real-world applications. In future, other types of planar springs can also be explored to enhance the nonlinearity. Also other possible magnet arrangements of the Halbach arrays can be further studied, such as circular Halbach arrays. In addition, the effect of the interface circuit of energy conversion and storage on the proposed EVEH deserves deep studies.

Declaration of Competing Interest

The authors declare that they have no known competing financial interests or personal relationships that could have appeared to influence the work reported in this paper.

Data availability

Data will be made available on request.

Acknowledgement

This work was supported by the National Natural Science Foundation of China (Grant No. 52377204).

References

[1] Muhammad A J, Kamran A, Qammer H A, Muhammad A I, Masood U R. Challenges, applications, and

future of wireless sensors in Internet of Things: A review. IEEE Sens J 2022; 22(6): 5482–5494.

[2] Wang P, Li W, Che L F. Design and fabrication of a micro electromagnetic vibration energy harvester, J Semicond 2011; 32(10): 104009.

[3] Knight C, Davidson J, Behrens S. Energy options for wireless sensor nodes. Sensors(Basel) 2008; 8(12): 8037–8066.

[4] Abdin Z, Alim M A, Saidur R, Islam M R, Rashmi W, Mekhilef S, Wadi A. Solar energy harvesting with the application of nanotechnology. Renew Sust Energ Rev. 2013; 26: 837–852.

[5] Alajingi R, Marimuthu R. A comprehensive review on small-scale thermal energy harvesters: Advancements and applications. Mater Today 2022; 66(3): 1552–1562.

[6] Anwesa M, Suraj P, K. Rabindra B, Tarapada R. Vibration energy harvesting: A review. J Adv Diele 2019; 9(4): 1930001.

[7] Yang T, Zhou S, Litak G, Jing X. Recent advances in correlation and integration between vibration control, energy harvesting and monitoring. Nonlinear Dyn 2023; 111: 20525–20562.

[8] Stephen N G. On energy harvesting from ambient vibration. J Sound Vib 2006; 293(1-2): 409–425.

[9] Khaligh A, Peng Z, Cong Z. Kinetic energy harvesting using piezoelectric and electromagnetic technologies-state of the art. IEEE Trans Ind Electronic 2010; 57 (3): 850–860.

[10] Bo L D, Gardonio P. Energy harvesting with electromagnetic and piezoelectric seismic transducers: unified theory and experimental validation. J Sound Vib 2018; 433: 385–424.

[11] Liang H T, Hao G B, Oskar Z O. A review on vibration-based piezoelectric energy harvesting from the aspect of compliant mechanisms. Sensor Actuat A-Phys 2021; 331(11): 112743.

[12] Sharma S, Kiran R, Azad P, Vaish R. A review of piezoelectric energy harvesting tiles: Available designs and future perspective. Energy Convers Manag 2022; 254: 115272.

[13] Farid U K, Muhammad U Q. State-of-the-art in vibration-based electrostatic energy harvesting. J Micromech Microeng 2016; 26(10): 103001.

[14] Afsharfard A. Application of nonlinear magnetic vibro-impact vibration suppressor and energy harvester. Mech Syst Signal Pr 2018; 98(1): 371–381.

[15] Arnold D P. Review of microscale magnetic power generation. IEEE T Magn 2007; 43(11): 3940–3951.

[16] Muscat A, Bhattacharya S, Zhu Y. Electromagnetic vibrational energy harvesters: A review. Sensors 2022; 22: 5555.

[17] Fan F R, Tian Z Q, Wang Z L. Flexible triboelectric generator. Nano Energy 2012; 1 328–334.

[18] Wang Z L. Triboelectric nanogenerators as new energy technology and self-powered sensors–Principles, problems and perspectives. Faraday Discuss 2014; 176: 447–458.

[19] Moss S D, Payne O R, Hart G A, Ung C. Scaling and power density metrics of electromagnetic vibration energy harvesting devices. Smart Mater Struct 2015; 24: 115290.

[20] Gardonio P, Bo L D. Scaling laws of electromagnetic and piezoelectric seismic vibration energy harvesters built from discrete components. J Sound Vib 2020; 476: 115290–115326.

[21] Elliott S J, Zilletti M. Scaling of electromagnetic transducers for shunt damping and power harvesting. J Sound Vib 2014; 333(8): 2185–2195.

[22] Seong J C, Jin H. K. Linear electromagnetic electric generator for harvesting vibration energy at frequencies more than 50 Hz. Adv Mech Eng 2017; 9 (10): 1–9.

[23] Zuo L, Scully B, Shestani J, Zhou Y. Design and characterization of an electromagnetic energy harvester for vehicle suspensions. Smart Mater Struct 2010; 19(4): 045003.

[24] Yang T, Xu H, Tang J, Zhou S. Exploring nonlinear degradation benefit of bio-inspired oscillator for engineering applications. Appl Math Model 2023; 119: 736–762.

[25] Phan T N, Bader S, Oelmann B. Performance of an electromagnetic energy harvester with linear and nonlinear springs under real vibrations. Sensors 2020; 20: 5456.

[26] Yang T, Zhang Y, Zhou S, Fan H, Zhang X. Wideband energy harvesting using nonlinear energy sink with bio-inspired hexagonal skeleton structure. Commun Nonlinear Sci 2022; 111: 106465.

[27] Phan T N, Bader S, Oelmann B. Performance of an electromagnetic energy harvester with linear and nonlinear springs under real vibrations. Sensors 2020; 20: 5456.

[28] Jia Y. Review of nonlinear vibration energy harvesting: Duffing, bistability, parametric, stochastic and others. J Intel Mat Syst Str 2020;31(7): 921–944.

[29] Mann B P, Sims N D. Energy harvesting from the nonlinear oscillations of magnetic levitation. J Sound Vib 2009; 319(1-2): 515–530.

[30] Gao M, Wang Y, Wang Y F, Wang P. Experimental investigation of non-linear multi-stable electromagnetic-induction energy harvesting mechanism by magnetic levitation oscillation. Appl Energy 2018; 220(10): 856–875.

[31] Daqaq M. Response of uni-modal Duffing-type harvesters to random forced excitations. J Sound Vib 2020;329(18): 3621–3631.

[32] Nguyen HT, Genov D, Bardaweel H. Mono-stable and bi-stable magnetic spring based vibration energy

harvesting systems subject to harmonic excitation: Dynamic modeling and experimental verification. Mech Syst Signal Pr 2019; 134(12): 106361.

[33] Sui L H, Dai X H, Zhao X L, Wang P H, Zhou H L. Design of nonlinear springs for wideband magnetic vibration energy harvester. Proceedings of the 6th IEEE International Conference on Nano/Micro Engineered and Molecular Systems, Kaohsiung, Taiwan, 20-23 February 2011.

[34] Sun S, Dai X H, Feng Z C, Ding G F, Zhao X L. Independent nonlinearity tuning of planar spring via geometrical design for wideband vibration energy harvesting. Sensor Actuat A-Phys 2017; 267(11): 393–400.

[35] Zhu D, Beeby S, Tudor J, Harris N. Vibration energy harvesting using the Halbach array. Smart Mater Struct 2012; 21(7): 075020.

[36] Ismardi A, Sugandi G, Lizarna M A. Design and simulation of double planar spring based on polyimide for electrodynamic vibration energy harvesting. J Phys: Conf Series 2019; 1170: 012061.

[37] Mallick D, Amann A, Roy S. A nonlinear stretching based electromagnetic energy harvester on FR4 for wideband operation. Smart Mater Struct 2015; 24(1): 015013.

[38] Jerzy M, Damian G, Grzegorz L, Piotr W, Daniil Y. Nonlinear dynamics of a new energy harvesting system with quasi-zero stiffness. Appl Energy 2022; 307: 118159.

[39] Spreemann D, Manoli Y. Electromagnetic vibration energy harvesting devices: architectures, design, modeling and optimization. Dordrecht: Springer, 2012.